

Pore system changes during experimental CO₂ injection into detritic rocks: Studies of potential storage rocks from some sedimentary basins of Spain



E. Berrezueta^{a,*}, L. González-Menéndez^a, D. Breitner^b, L. Luquot^c

^a Instituto Geológico y Minero de España, Oviedo, Spain

^b Centre for Energy Research, Hungarian Academy of Sciences, Budapest, Hungary

^c Institute of Environmental Assessment and Water Research (IDAEA-CSIC), Barcelona, Spain

ARTICLE INFO

Article history:

Received 31 December 2012

Received in revised form 17 April 2013

Accepted 27 May 2013

Keywords:

CO₂ capture and storage

Supercritical CO₂

Pore-evolution system

ABSTRACT

The effects of experimental injection of CO₂ into potential deep sedimentary formations are investigated, focusing on detritic rocks with interconnected pore networks. This approach consisted in the qualitative and quantitative determination of mineralogical and textural changes in selected sedimentary rock samples after injection of supercritical CO₂ ($P \approx 75$ bar, $T \approx 35$ °C, 12–970 h exposure time and dry conditions). The mineralogy and texture were studied before and after the injection by optical and scanning electron microscopy, and quantification was done with digital image analysis. The studied rocks were sampled from different sedimentary basins in Spain and consist of feldspar sandstones with similar mineralogy but different textures (homogeneous vs. heterogeneous).

The results obtained in the CO₂-treated samples indicate a porosity increase ($\Delta n = 3.75\%$) and a qualitative permeability rise. Intergranular clay matrix detachment and partial removal from the rock sample (due to CO₂ input/release drag and electrical-polarity forces) are the main processes that explain the porosity increase. In contrast, carbonate cements were stable and no substantial changes were observed. Additional textural changes were minor and consisted on variations in the roughness of grain-pore contacts, pore shape and aspect ratio. Primary texture of the rock subjected to CO₂ injection is an important factor and seems to enhance textural/mineralogical changes in heterogeneous systems.

These results simulate the CO₂ injection nearest to the injection well and indicate that, in this environment, where CO₂ push out the brine fluids and interacts with rocks in dry conditions, several mineralogy/texture re-adjustments take place. Consequences derived from these changes are variable. Possible porosity and permeability increases could facilitate further CO₂ injection but textural re-adjustment could also affect the rock physical properties.

© 2013 Elsevier Ltd. All rights reserved.

1. Introduction

One of the major environmental and climatic issues nowadays is to reduce the atmospheric CO₂ concentration by capture and storage into geological formations (CCS). Deep geological storage into rock porous formations is considered the most appropriate strategy for CO₂ sequestration (Izeg et al., 2008; Benson and Cole, 2008; Gauss, 2010) and injectivity is a key technical and economical issue for CCS projects (Bacci et al., 2011). The viability of the CO₂ injection depends mainly on the porosity and permeability of the storage rocks. Other further consequences of the CO₂ interaction with host rock such as dissolution–precipitation of minerals

are also important (e.g., Ross et al., 1982; Sayegh et al., 1990 and Saeedi et al., 2011).

Both theoretical and experimental studies have been done to study the CO₂–rock interactions at the deep storage conditions. Most of the experimental studies are designed to simulate the injection of CO₂, mixed with brine fluids, in rocks at P–T conditions of deep storage environment. The results in many of these experiments were an increase in the porosity/permeability of the storage rock caused by partial dissolution of the carbonate components (mainly calcite) (Perkins & Gunter, 1995; Svec and Grigg, 2011; Rochelle et al., 2004; Egermann et al., 2005; İzgeç et al., 2005; Izeg et al., 2008; Gunter et al., 2008, Luquot and Gouze, 2009; Desbois et al., 2011). However, other set of experiments has shown porosity decreases due to the initial dissolution of carbonates followed by secondary precipitation/mineralization (Kaszuba et al., 2003; Cailly et al., 2005; Kaszuba et al., 2005; Mito et al., 2008; Sterpenich et al., 2009; Luquot and Gouze, 2009).

* Corresponding author. Tel.: +34 609381623.

E-mail addresses: e.berrezueta@igme.es, geoedgar@yahoo.com (E. Berrezueta).

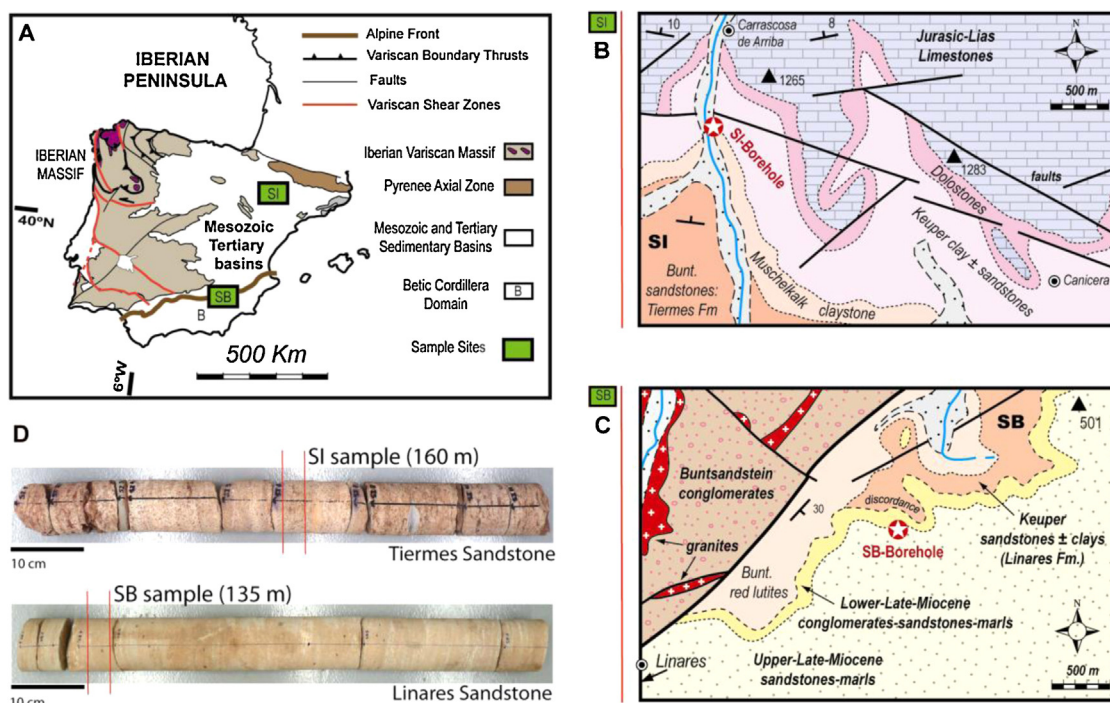


Fig. 1. Location (A) and regional geology of the areas selected for the borehole and sample collection. (B) SI sandstone sample location (Lendínez and Muñoz, 1989). (C) SB sandstone sample location (Azcárate et al., 1974). (D) Core samples representative for the two sandstones formations (Tiermes and Linares Sandstone).

On the other hand, only a few researches have studied the CO₂ injection into potential storage rock formations under dry conditions (Vickerd et al., 2006). This is probably because the environment of injection is mainly envisaged as injected CO₂ mixed with brine fluids in sandstones rocks. However, in near-well injection sites, the supercritical CO₂ laterally displaces the brine and occupies the pore framework of the rocks, in either dry or near-dry conditions (Burton et al., 2008; Luquot and Gouze, 2009; Gauss, 2010). Therefore, in this specific case, dry CO₂ interaction with the storage rocks is a realistic scenario that takes place in the initial injection stages. Some theoretical studies on dry CO₂–rock interactions (Gauss et al., 2008; Gauss, 2010) and also experimental results (Sterpenich et al., 2009) indicate absence of reactions and consequently negligible textural–mineralogical changes. This is explained by the lack of H₂O in the system that prevents dissolution/precipitation and any kind of mineral–chemical reactions.

Our research is focussed on the experimental dry injection of supercritical CO₂ into selected rock samples representative of potential storage reservoirs in Spain. The selected P–T conditions and run-times of our experiments aim to reproduce the storage-rock dry environment adjacent to the injection borehole, and investigate the textural–mineralogical and petrophysical changes in selected rock samples before and after experimental injection of supercritical CO₂. Once target pressure and temperature were reached inside the reactor chamber (CO₂ supercritical conditions) no CO₂ flow occurred within the chamber (isolated conditions).

The main results of our research indicate that physical ± chemical changes related to CO₂ input induce textural re-adjustments resulting in increases (or at least changes) in the micro porosity and permeability of the storage rocks.

2. Methodologies and initial condition study

The working steps in the study of mineralogical and textural changes in experimental CO₂ injection into detritic rocks included:

- Selection of representative samples for study (geological setting).
- Petrography characterization studies. Textural and mineralogical description of the samples by optical microscopy, SEM and digital image processing in rock thin sections (~30 μm thick).
- CO₂ injection at selected conditions (supercritical CO₂: 75 bar and 35 °C) in the Hyperbaric Chamber: (a) Stage 1 – CO₂ pressurized injection (3 h); (b) Stage 2 – CO₂ pressurized stabilization (12–970 h) and (c) Stage 3 CO₂ – pressure release (3 h).
- After-injection textural and mineralogical study and comparison with the untreated sample. Although the thin sections and SEM samples do not exactly correspond to the same sample surface, both are located very close (a few mm) in the original source-sample.
- Detailed optical microscope study and quantification of the mineralogical and textural variability were performed in the untreated samples to verify that any change observed in the experiments was due to the CO₂ effect and not to the possible original heterogeneity.
- Finally, results of mineralogical quantification were evaluated using statistical tests.

2.1. Samples: geological setting and petrography

Two sandstone geological formations, potentially suitable for CO₂ sequestration, were selected for this study. The studied rock samples were immature (sediments located close to its source area, short transport distance) greywacke/arkosic Triassic sandstones from the Guadalquivir basin in SE Spain (SB: Linares-Manuel Fm.) and the Iberian Ranges in N-NE Spain (SI: Tiermes Fm.) (Fig. 1). These formations have significant porosities and permeabilities, are partially sealed by impermeable formations, and are unaffected by faults and fractures related to recent seismic activity. The mineralogy of the studied sandstone formations is similar: quartz (Qtz), K-feldspar (Kfs), phyllosilicates (e.g., sericite and other clays), carbonates and, in minor abundance, biotite (Bt), muscovite (Ms), plagioclase (Pl), apatite (Ap), zircon (Zrn) and Fe-

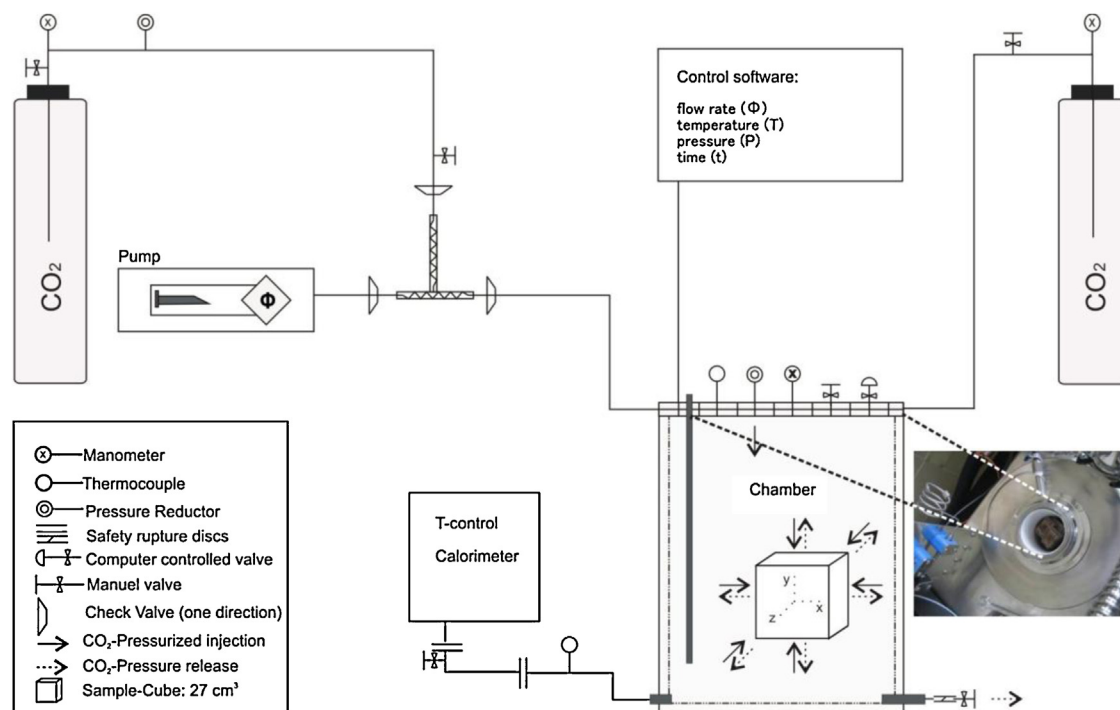


Fig. 2. Diagram of the experimental setup: reactor system used for the pressurized CO₂ injection. See text for explanation.

oxides. The phyllosilicates form the rock matrix and carbonates constitute cements. In some sample domains sericitic clays and Fe-rich (hematite) particles form a mixture of clay matrix-iron-rich cement. The clay matrix/carbonate ratio can be variable within a single sample. The main difference between the two rock formations is the texture. The Tiermes Sandstone (SI), compared to Manuel Sandstone (SB), is more heterogeneous and less well sorted with higher porosity and permeability produced by an interconnected framework of micro-channels. In contrast, Manuel Sandstone (SB) is more homogeneous and shows a better sorting. Its porosity does not show micro-channel structures and is more evenly distributed (detailed in Section 3).

2.2. Experimental setup (reactor system)

The experimental setup applied during this experiment is based on similar systems described by Luquot and Gouze (2009) and Luquot et al. (2012). However, some modifications have been performed due to the different characteristics of the target rock system. Sample material (rock type and representative sample size), geological environment (pressure, temperature and salinity) and technical equipment (materials for camera, software, pumps, etc.) were all considered for the setup of the experimental device (Fig. 2) and for the run conditions. The CO₂ injection was performed into cubic-shaped samples (2 cubes of 27 cm³ from each sandstone sample) using a constrained hyperbaric chamber-reactor where the dry CO₂ was pumped at pressures and temperatures of 75 bar and 35 °C, respectively. These conditions reproduce host rock formations at depth of ca. 800 m. The time of CO₂ sample exposure varied from 12 to 970 h (no CO₂ flow inside the chamber). The system reactors (Fig. 2) have two CO₂ cylinders (standard-industrial CO₂ to 45 bars) that are linked to the other elements of the system by steel connectors (diameter: 5 mm). The second CO₂ cylinder is connected to a piston pump that operates with a flow of 0.01 g/s. When the required pressure conditions (75 bar) decrease (due to possible leaks) then this pump will inject CO₂ to keep the pressure within the desired values. The piston pump needs a CO₂ initial pressure of

10 bars in order to inject CO₂ into the Hasteloy Steel chamber (6L), therefore, the pressure between the piston pump and the second CO₂ cylinder has to be decreased by a pressure manometer from 45 to 10 bar. The chamber is coated with polytetrafluoroethylene (PTFE) internal protection that protects its interior. At the bottom of the chamber, a calorimeter controls the internal temperature. The calorimeter and the pump are linked to the chamber by pressure and temperature sensors and are connected to the central computer. The time of filling and emptying of the chamber with supercritical CO₂ was the same (3 h): This is the time required to reach the target pressure and temperature values (P: 75 bar and T: 35 °C inside to reactor), from the initial ambient conditions. This same amount of time was used to get back to the ambient conditions at the end of the experimental test. The applied software HEL 5.1 allows the remote control of the system (any change in the experiment conditions) through the development of specific macros (pressure, temperature, time) in real time. The system has been designed to have the possibility for adding other modules such as brine cylinders, pump for brines, pH sensor, etc. All the experimental runs for this study were carried out in the Laboratories of the Geological Survey of Spain (IGME) in Tres Cantos, Madrid.

2.3. Techniques applied to the studied samples

In order to study qualitatively the textural and mineralogical changes due to experimental CO₂ injection, optical microscopy (OpM) (Leica DM 6000 polarization microscope (magnification of 10×)) and scanning electron microscopy (SEM) (JEOL 6100 SEM, using W-Filament, acceleration voltage of 20 kV and Inca Energy-200 software) were used. The investigations were accomplished by direct observation and comparison between CO₂-untreated and CO₂-treated samples. The optical microscopic studies were performed in Geological Survey of Spain (Leon Unit), the SEM studies at the Scientific-Technical Services of University of Oviedo and the quantification using digital image analyses (DIA) in the Geological Survey of Spain (Oviedo Unit).

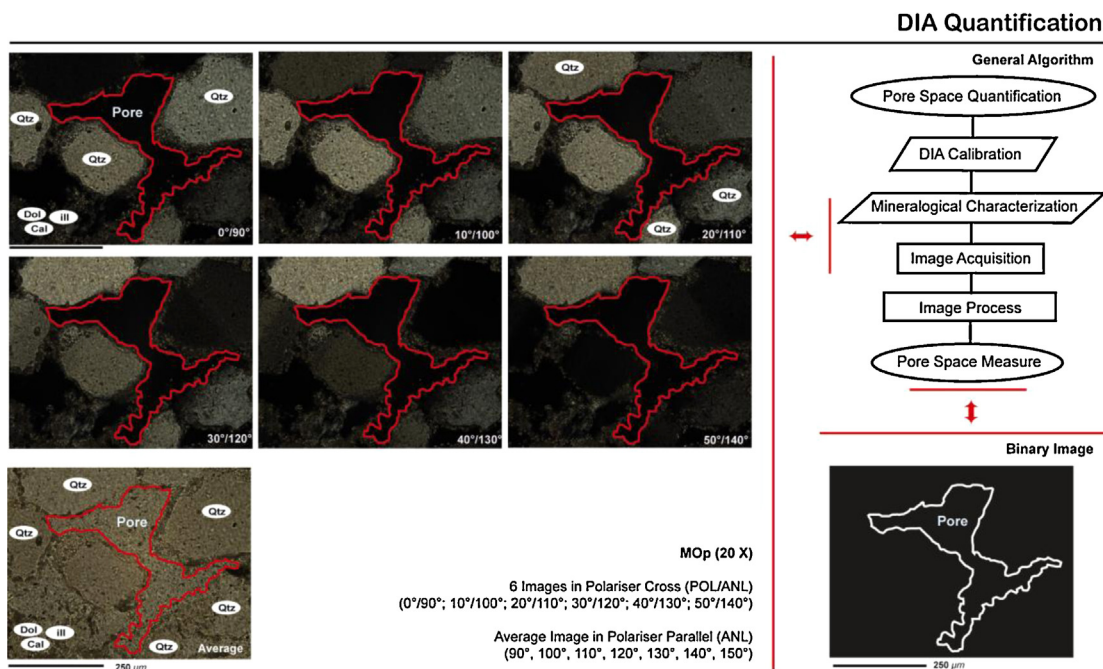


Fig. 3. DIA quantification of pore system (mineral images acquired, general algorithm of DIA and binary image with pore).

In order to quantify important petrographical and mineralogical parameters (area, roughness of minerals/pore boundaries, fractal dimension, circularity of minerals/pores and porosity) DIA using *Aphelion 3.2* and *Image Pro Plus 7.0* software was applied (Berrezueta and Castroviejo, 2007; Berrezueta et al., 2012). For mineral and porosity classification (Fig. 3) 12 different images scenes (6 in cross polarizers and 6 in parallel polarizers) of the same mineral information (moving synchronized polarizer and analyser with 10 degrees) were acquired and included them in specific macros developed in this study (pore quantitative characterization). The results of DIA before and after supercritical CO₂ injection were tested by *t*-student and Mann–Whitney tests using *SYSTAT*® (13.0) and *MINITAB*® (15.0) commercial software packages. The main objective of these statistical studies was to determine the existence/absence of different populations of mineral textures and pore shapes between the pre- and post-injection samples and verify whether these differences, if any, were significant. Software references are in Appendix 1.

3. Results

The results obtained, for homogeneous SB sandstones and SI heterogeneous sandstones (Figs. 4–6), before and after the experimental injection of CO₂, is outlined as an evolution of the textural and mineralogical features from the untreated samples to the treated samples.

3.1. Untreated homogeneous sandstone (SB: Linares-Manuel Fm)

This sandstone has both carbonate cement and clay matrix. The texture is characterized by a general good sorting (0.35–0.5 index of Pettijohn et al. (1973)) with an evenly distribution of the major mineral constituents (mainly quartz) and is classified as homogeneous sandstone (Fig. 4). In some specific domains (thin section scale) a subtle mineral grain orientation was observed. The grain size is fine sand (<0.5 mm). The angularity of the mineral grains is moderate (sub-rounded to sub-angular). The modal content of matrix (clay minerals) is about 15%, corresponding to immature

sediments. The modal porosity estimated through modal counting (counts of 400–500 points per thin section) is ≈5% and its interconnection (permeability) seems limited in the 2D thin section plane. The mineralogy (see Appendix 2 for mineral abbreviations) consists of Qtz (40%)+feldspars (12%) (Kfs+Pl)+Cal/Dol (15%). As accessory minerals (≈6%) there are detrital Ms±Chl±iron oxides (hematite and limonite: Fe₂O₃–Fe₂O₃ × nH₂O)+Zrn+Tur. Rock fragments also occur with a modal abundance of ca. 7% and a size close to the main mineral grains (Qtz±feldspars). These rock fragments are composed, in most cases, of metamorphic Qtz sutured grains. The matrix minerals are probably sericite and other clays±Chl, whereas the carbonate cement is made by Cal±Dol. This sample can thus be classified as a feldspathic sandstone or sub-arkose (Folk, 1974) (Fig. 4a). The SEM study of this sample has shown in more detail the clay matrix composition: smectite clays (≈montmorillonite)±illite or secondary Ms as the main sericite clay (±Cal±Dol±Kfs±Qtz). Also a more detailed observation of the pore structure was performed showing that the main porosities are, in some cases, located adjacent to the major mineral grains (contacts between major mineral grains and matrix/cement) whereas in other cases porosities are within the clay matrix. The approximate size of these pores is ca. 5–10 µm (Fig. 4a). Regarding the main mineral grains (Qtz, feldspars, calcite), these have usually sharp and clean faces/surfaces in contact with the matrix/cement mineral grains (1–5 µm, Fig. 4). The intergranular space, observed both in the optical microscope and SEM, is commonly filled with cement or matrix in such a way that the major mineral grains do not contact each other in many of the observed cases (Fig. 4a).

The quantification by DIA was applied on images acquired by Optical Microscopy (30 images per transmitted section). The DIA has allowed us to quantify several interesting parameters related to the morphology, size and space distribution of the pore network. The porosity (*n*₁) measurement was 4% (Table 1) and a pore distribution by size range (area) corresponding to a logarithmic distribution function. For the application of statistics tests (Table 2, *t*-student or Mann–Whitney) it was necessary to convert the original data to a normal distribution (*X*_{SB}: 3,49; *σ*_{SB}: 0,41), using a log transformation.

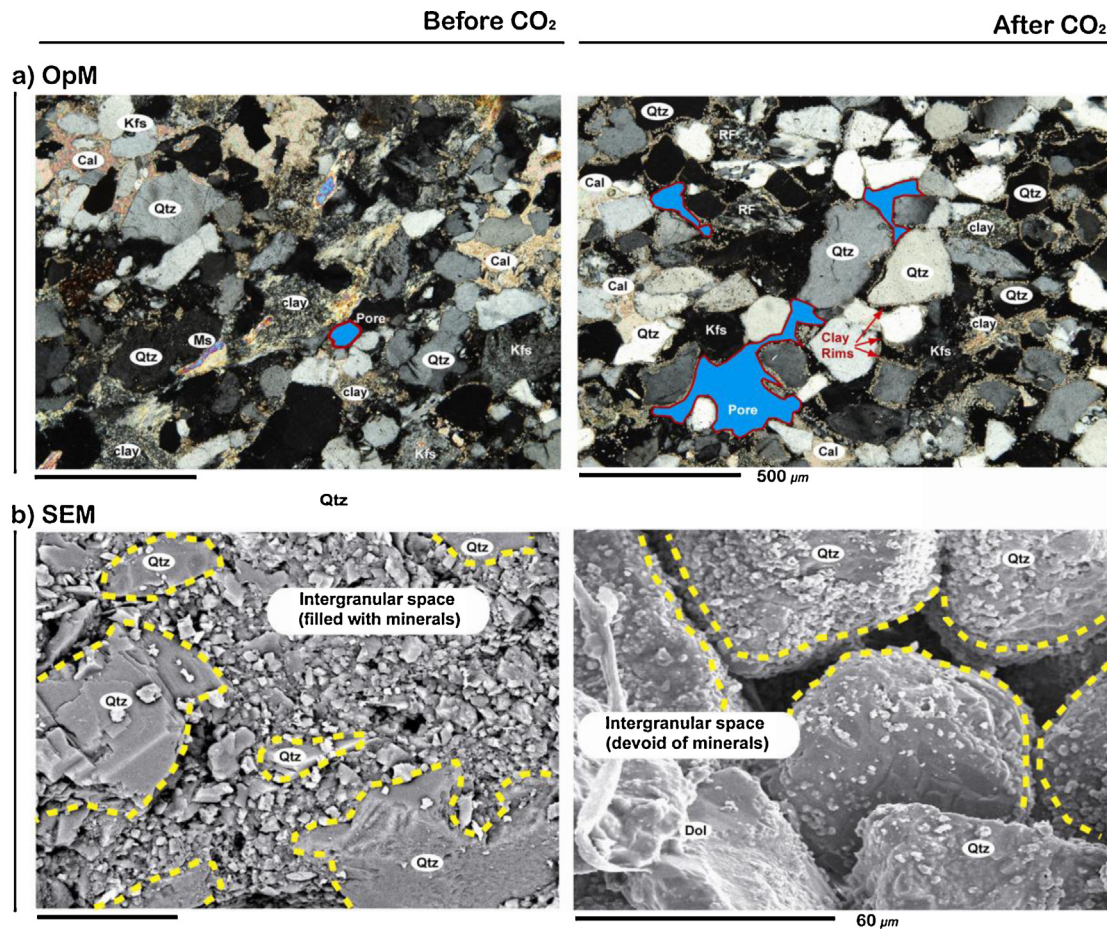


Fig. 4. Textural–mineralogical characterization of Linares sandstone (SB): (a) optical transmission (cross polarizers) images (OpM) of the rock sample before S.C. CO₂ injection and after S.C. CO₂ injection. (b) scanning electron microscopy (SEM) images of the samples before and after S.C. CO₂ injection.

Table 1

Total porosity of sandstone sample (SI and Sb/pre and post CO₂) measured by DIA.

DIA: measures	Pore area (µm ²)	Mineral area (µm ²)	Total porosity (ni) (%)	Porosity Variation (Δn) (%)
SB pre CO ₂	784,982	19,624,550	4	3
SB post CO ₂	1,373,718		7	
SI pre CO ₂	470,989	11,774,730	10	4
SI post CO ₂	824,231		14	

Table 2

Paired *t*-Student's (for data log, using N1 population) and Mann–Whitney (for data log) of different pore-parameters measured (pixels) through DIA techniques.

$\alpha = 0.1$	N1	Pre-CO ₂ inject Mean	N2	Post-CO ₂ inject Mean	<i>p</i> -Value <i>t</i> -Student's	<i>p</i> -Value Mann–Whitney	Interpretation
SB pore area	468	3.4910	698	3.5540	0.009	0.0015	Increase
SB Pore aspect	468	0.2820	698	0.2756	0.472	0.7464	No change
SB pore rough	468	0.0738	698	0.0705	0.006	0.0057	Decrease
SB pore circul.	468	0.6427	698	0.623	0.109	0.1642	No change
SI pore area	544	4.3510	835	4.4470	≈0	0.0001	Increase
SI pore aspect	544	0.2674	835	0.3034	≈0	0.0001	Increase
SI pore rough	544	0.0611	835	0.0546	≈0	0	Decrease
SI pore circul.	544	0.5413	835	0.5718	0.006	0.0265	Decrease

3.2. CO₂-treated homogeneous sandstone (SB: Linares-Manuel Fm)

The sample exposed to 970 h of S.C. CO₂ develops distinctive textural and mineralogical features compared to the untreated sample. In the thin section scale (10×–40× magnification) the most significant changes, are the increase of porosity, the absence of an important volume of the clay matrix and the common development

of thin clay mineral (sericitic) rims (ca. 10–20 µm thickness) around the main mineral grains, mainly Qtz (Fig. 4b). At SEM (500×–2500× magnification) the most important feature is the above-mentioned absence of a significant amount of the clay matrix. The main mineral grains, surrounded by the clay matrix in the untreated samples, now form a grain framework in which many grains are in physical contact with each other. This absence of clay matrix is the main cause of porosity increase as observed in the SEM images (Fig. 4b).

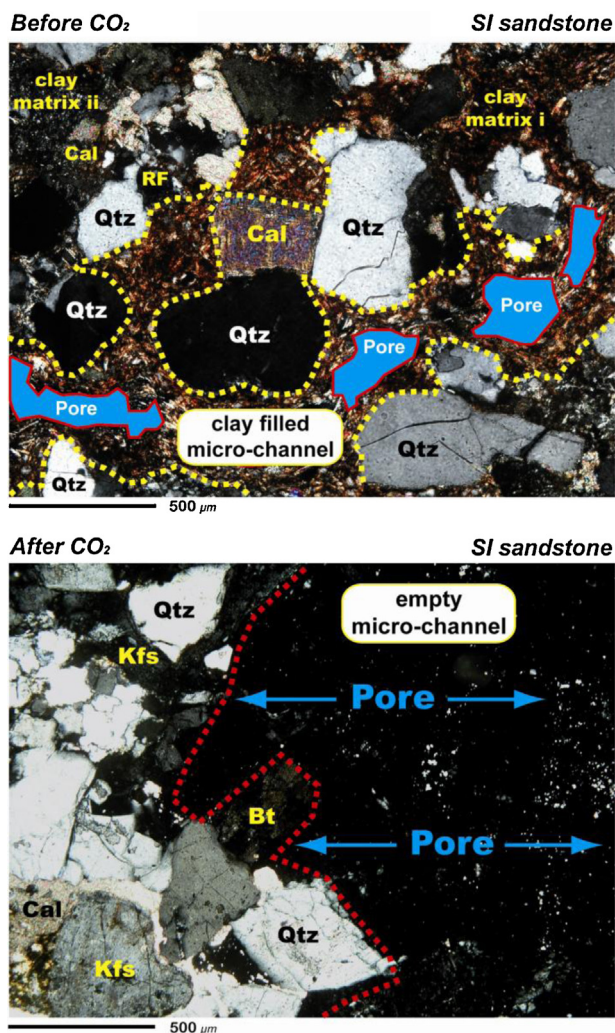


Fig. 5. Microphotographs of the micro-channelled structure in the SI (Tiermes) sandstone (OpM). In the rock sample, before the CO₂ injection, micro-channels are partially filled with a mixture of clay matrix ± other minerals (mainly Qtz and iron oxides: the main quartz grains located at the boundaries of micro channels were probably polished by the fines mobilized due to the CO₂). Clay minerals also occur in other domains of the sample unrelated to micro-channels (clay matrix i). After the CO₂ injection, clay matrix removal, partially or totally emptied the micro-channels.

Also observed in the SEM images, over the external surfaces of the main mineral grains, a conspicuous and discontinuous coating of very small mineral grains (ca. 1–10 µm size) occur probably composed of clay minerals (Fig. 4b). These small mineral grains attached to the major mineral surfaces, could correspond with the rims of clay grains observed in the optical microscope. Regarding the carbonate cement, no major differences have been found between treated and untreated samples. This could indicate that the carbonate cement is physically more stable than the clay matrix (further details in Section 4).

Quantification by DIA method was applied in conditions similar to those used in the untreated sample. The quantification of porosity (n_2) was 7% (Table 1). The pore-size variation in the thin sections shows a logarithmic distribution function. For the application of statistics tests (Table 2, *t*-Student or Mann–Whitney) it was necessary to convert the original data to a normal distribution (X_{SB} : 3.55; σ_{SB} : 0.40), using a log transformation. Importantly, the number of pores increased by 49% compared to untreated sample. These techniques of image quantification applied to the pore area allow estimations of porosity increases (increase of pore-area in the thin section) of Δn : $n_2 - n_1 \approx 3\%$.

3.3. Untreated heterogeneous sandstone (SI: Tiermes Fm)

In this sandstone the main mineral grains are sub-rounded and poorly sorted. The rock has both matrix clay (ca. 7%) and more abundant carbonate cement (ca. 13%). Since the amount of matrix content is over 5%, the sandstone is classified as immature. The distribution of the carbonate cement is homogeneous, whereas the clay matrix occurs mainly along micro-channels that cut across the rock. Micro-channels are an important textural feature (Fig. 5a). These are several mm long (ca. 4 mm) and about 0.5–1 mm of width on average. Its orientation is variable; do not follow straight linear patterns indicating no relation to previous micro-fractures. These micro-channels cause the high porosity of the sample. These interconnected voids are partially filled with a mixture of clay matrix + carbonates + Qtz ± iron oxides, probably limonite and hematite. The whole space volume of these conduits (primary porosity) was once totally filled with the mentioned mineral mixture. Possible late diagenetic/freatic fluid circulation generated partial dissolution of this mineral mixture and the present secondary porosity (Fig. 5a). Regarding mineralogy, the main SI phases are Qtz (32%) + Feldspars: [Kfs ± Pl] (21%) + carbonate cement [Cal/Dol] (13%) + clay matrix: smectite ± sericitic clays (7%). Rock fragments account for ≈5% of the rock whereas accessory minerals are <1.5% and include detrital Ms + Bt + Tur + Chl ± Fe-oxides ± Tur ± Zrn. The rock is classified as a greywacke (Folk, 1974). The clay minerals can occur in two different ways: (i) mixed with Qtz + carbonates ± iron oxides in the micro-channels (clay matrix (i) in Fig. 5a). In this case the clay minerals show oriented shapes and fluidal texture that could be related to past fluid circulation processes; (ii) matrix clays can occur, less commonly, scattered through the rock, unrelated to micro-channels, and partially replacing primary phases such as feldspars (clay matrix (ii) in Fig. 5a). The open porosity is concentrated within the micro-channels, and can be quite high in some domains (up to ~18%). The lateral interconnection of this porosity is high in the 2D plane of the thin section (Figs. 5 and 6). At the SEM scale the mineral phases mentioned were qualitatively analyzed, showing that the clay minerals are probably smectite like clays (≈montmorillonite) ± illite ± secondary muscovite or sericite (Fig. 6a). Other identified phases are salt minerals that were detected by its qualitative composition (K, Mg, Cl, Na) and could consist of associations of halite (NaCl) – carnalite (KMgCl₃·6H₂O). These salts appear to be part of the matrix, together with other clay minerals such as montmorillonite, illite and sericite. Due to the scale of the SEM observation, the mentioned micro-channels were not identified but most probably this association of salts + clay minerals forms part of the mineral mixture that partially fills the micro-channels. Other SEM observed features are the clean and straight grain mineral surfaces and contacts with other mineral grains and with the cement/matrix.

DIA quantification of pore system was carried out on 18 images of a thin sheet. The measured total porosity (n_1) was 10% (Table 1) with a pore distribution curve of a Logarithmic distribution function. For the application of statistics tests (Table 2, *t*-Student or Mann–Whitney) it was necessary to convert the original data to a normal distribution (X_{SB} : 4.35; σ_{SB} : 0.40), using a log transformation.

3.4. CO₂-treated heterogeneous sandstone (SI: Tiermes Fm)

After the S.C. CO₂ injection into the sample (exposition: 970 h), several significant changes were observed. The most noteworthy aspect that can be seen at the optical microscope is the near complete absence of the mineral mixture (clays + carbonates + Qtz + Fe-oxides) that partially filled the micro-channels (Figs. 5 and 6). Some remains of this mixture can still be observed attached to the major mineral surfaces open to the

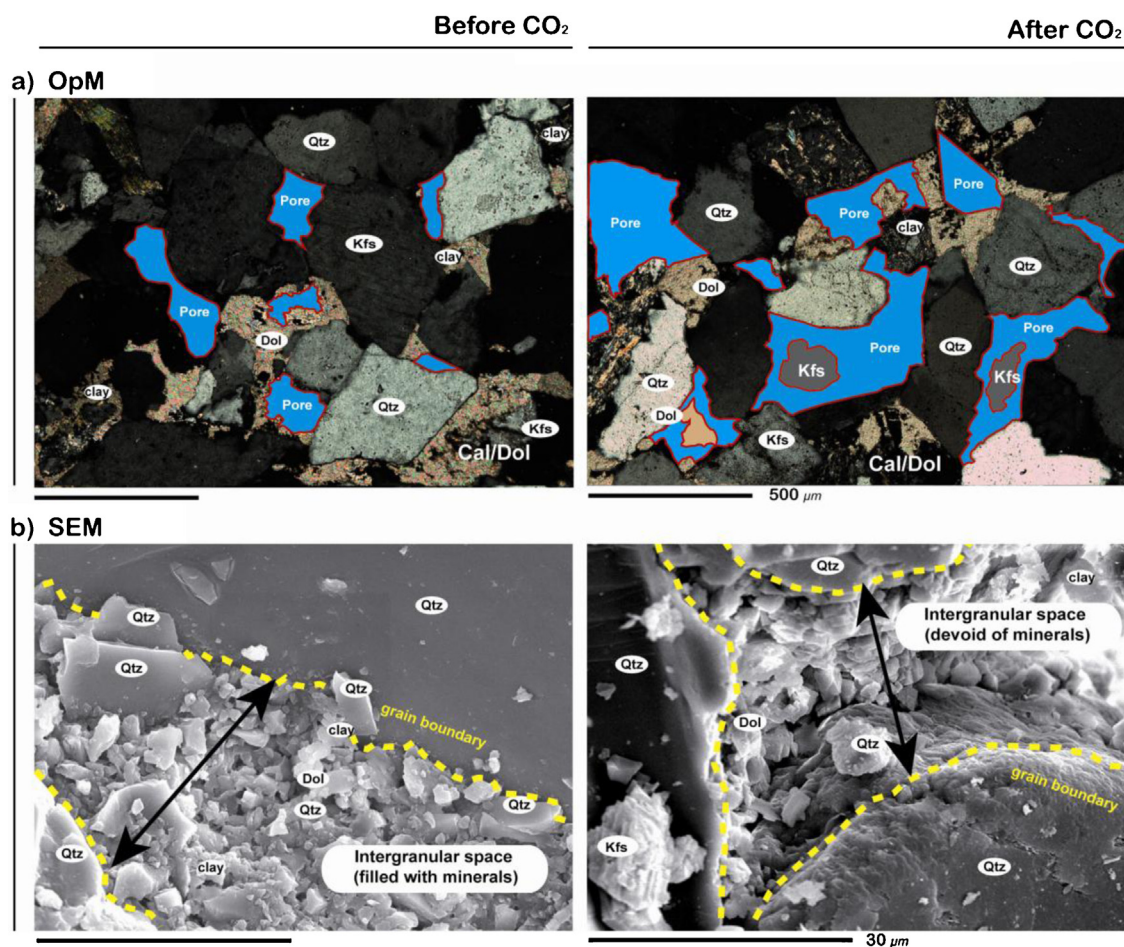


Fig. 6. Textural–mineralogical characterization of Tiermes sandstone (SI): (a) optical transmission (cross polarizers) images (OpM) of the rock sample before S.C. CO₂ injection and after S.C. CO₂ injection. (b) scanning electron microscopy (SEM) images of the samples before and after S.C. CO₂ injection. After the CO₂ injection, clay matrix removal, partially or totally emptied the micro-channels. The main Qtz grains located at the boundaries of micro channels were probably polished by the fines mobilized due to the CO₂.

channels. In other domains, micro-channels have been completely emptied after the CO₂ injection and release (Fig. 5b). This mineralogical/textural change causes a significant increase of porosity. On the other hand, the clays that were originally scattered through other parts of the rock, less related to micro channels, remained more stable. The carbonate cement also remained stable and no difference was observed compared to the untreated sample. At the SEM scale (Fig. 6b) we observed a possible increase of salty minerals (K–Mg–Cl salts) and a decrease of the modal amounts of clays and sericitic clay minerals. Although these changes seem to be slight and difficult to quantify, they are well correlated with the optical microscopy observation of micro-channel matrix modal decrease. Some mineral grain edges and boundaries appear to be different (more polish surfaces: Fig. 6b) compared to the untreated sample, but these differences are very subtle and therefore difficult to interpret. One significant feature is the presence of small mineral grains partially covering some of the major mineral surfaces (mainly Qtz grains). These small sized minerals (ca. 1–5 μm) are clays ± Cal ± micro Qtz ± salts, and, as in the case of the SB homogeneous-treated sandstone, could be residual matrix minerals that remained stucked to the major mineral surfaces.

Quantification by the DIA method shows that porosity (n_2) is 14% (Table 1). The distribution curve of the porosity according to their size ranges was a Logarithmic distribution function. For the application of statistics tests (Table 2, *t*-Student or Mann–Whitney) it was necessary to convert the original data to a normal distribution

(X_{SB} : 4.44; σ_{SB} : 0.44), using a log transformation. The number of pores was increased by 53% compared to untreated sample. The digital image quantification applied to the pore area indicates a porosity increase (Δn : $n_2 - n_1$) of ca. 4% after the CO₂ treatment.

4. Discussion

4.1. Causes of the observed changes

The observed changes in the studied samples are due to the CO₂ input and can be of importance in the realm of the injection well where the interaction of the CO₂ and the rock takes place in dry, or almost dry, conditions (Kharaka et al., 2006; Gauss, 2010). Any changes in mineralogy–porosity (Figs. 4–6; Tables 1 and 2) could change the rock texture framework and could affect the injection well and its closest environment and hence the injection efficiency. Our experimental investigation indicates that the main changes observed from the untreated to the treated–CO₂ samples are: (i) differences in the matrix clay content that consist on a modal clay reduction in the treated samples with a corresponding porosity increase, (ii) relative stability of the carbonate cement and (iii) variations in the pore morphology (Fig. 7) such as surface area, aspect ratio, roughness and circularity.

(i) Clay matrix reduction and porosity–permeability increase

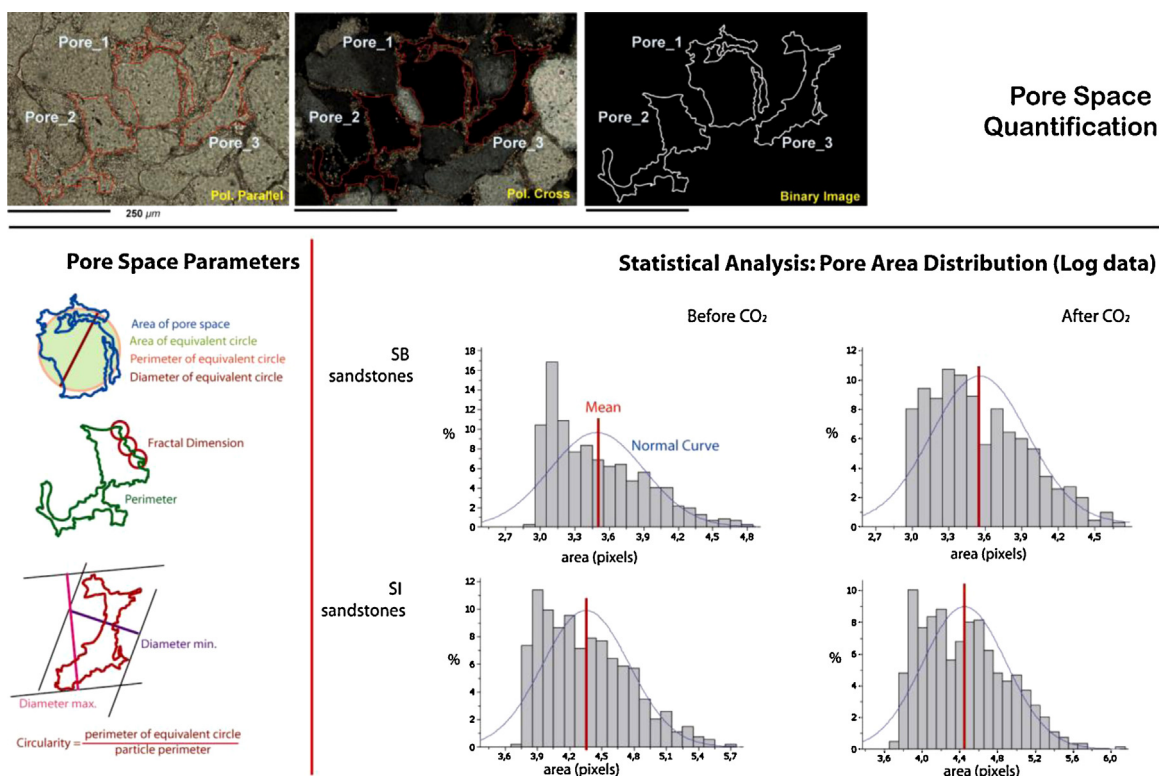


Fig. 7. DIA quantification of pore system (pore identification, pore parameters measured and statistical analysis applied).

Since the mineralogy of both rock samples (SB and SI) is very similar, the original rock texture is probably what promotes the varied effects when CO₂ is injected. In both study cases a common consequence is evident: clay matrix removal + pore increase, leading to a permeability increase. Nevertheless, in the case of the homogeneous sandstone (SB) most of the rock volume is affected by clay removal + porosity increase (CO₂ percolates through the homogeneously distributed pore network), whereas in the case of the heterogeneous sandstone (SI) there are ample zones of rock volume where the general texture is less affected and the major changes (clay removal + pore increase) are located within the micro-channel domains or close to them (CO₂ percolates through the heterogeneously distributed pore network). This could be explained by a preferential CO₂ flux into these channels, because of its lower stress resistance, focusing most of the CO₂ input into this channelized-pore network, and thus leaving ample rock domains with less CO₂ interaction.

How the clay matrix becomes effectively removed from the rock sample is an important question because it deals with the storage rock stability when supercritical CO₂ injection takes place. We consider that the pressurized CO₂ input and CO₂ expansion during pressure release promotes a mechanical drag force able to break the physical bonds of the clays with other clays (Vickerd et al., 2006). Additional effects of the CO₂ input to be considered are: (i) CO₂ diffusion into the clay layered structure causing changes in the molecular clay-water chemistry (increasing local pH), leading to polarity changes in the internal electrical forces (Van de Waals attraction, double layer repulsion) and eventually resulting in intra-particle/interparticle repulsion (Fripiat et al., 1974; Andreani et al., 2008; Pèpe et al., 2010; Espinoza and Santamaría, 2012). (ii) CO₂ diffusion into the clay layered structure and gas expansion during pressure release that causes clay layer breaking and generation of delaminated nanocomposites or nanoclays (Horsch et al., 2006).

All these considerations allow us to build a conceptual model for the experimental CO₂ injection (Fig. 8a–e). The CO₂ input and

release would have affected the clay matrix particles in several different ways that finally led to a detachment and partial re-adjustment of most of the clay matrix volume (except for part of the clays fixed to major mineral grains). These effects could have resulted in a partial loose of the matrix leading to the general observed absence of clay matrix:

Stage 1 – CO₂ pressurized injection:

- Initial CO₂ input would percolate through the rock pore system generating a mechanical drag force that was probably effective in breaking some of the inter clay-particle binds and probably causing clay accumulations near pore throats (Fig. 8b).

Stage 2 – CO₂ pressurized stabilization:

- This stage spans through most of the experimental run (~1000 h). During this time, CO₂ also diffused into the intra-layered clay structure causing electrical-polarity changes that led to an increase of repulsion and internal clay breakdown as observed in other investigations (references above) (Fig. 8c). This is mainly effective in the clay minerals that can hold molecular water between T–O or T–O–T layers (T: tetrahedral; O: octahedral), such as the smectite like clays (i.e., montmorillonite) but probably not in the sericite clays (secondary Ms or illite) where the interlayered cations (K) could prevent both H₂O and CO₂ diffusion into the structure.

Stage 3 – CO₂ pressure release + expansion:

- Intra-clay particle CO₂ expansion during pressure release would also promote further internal clay layer breakdown and generation of nanoclays that would allow us to explain the fine clay-like particles attached to the surfaces of major minerals after CO₂ exposure (Fig. 8d).

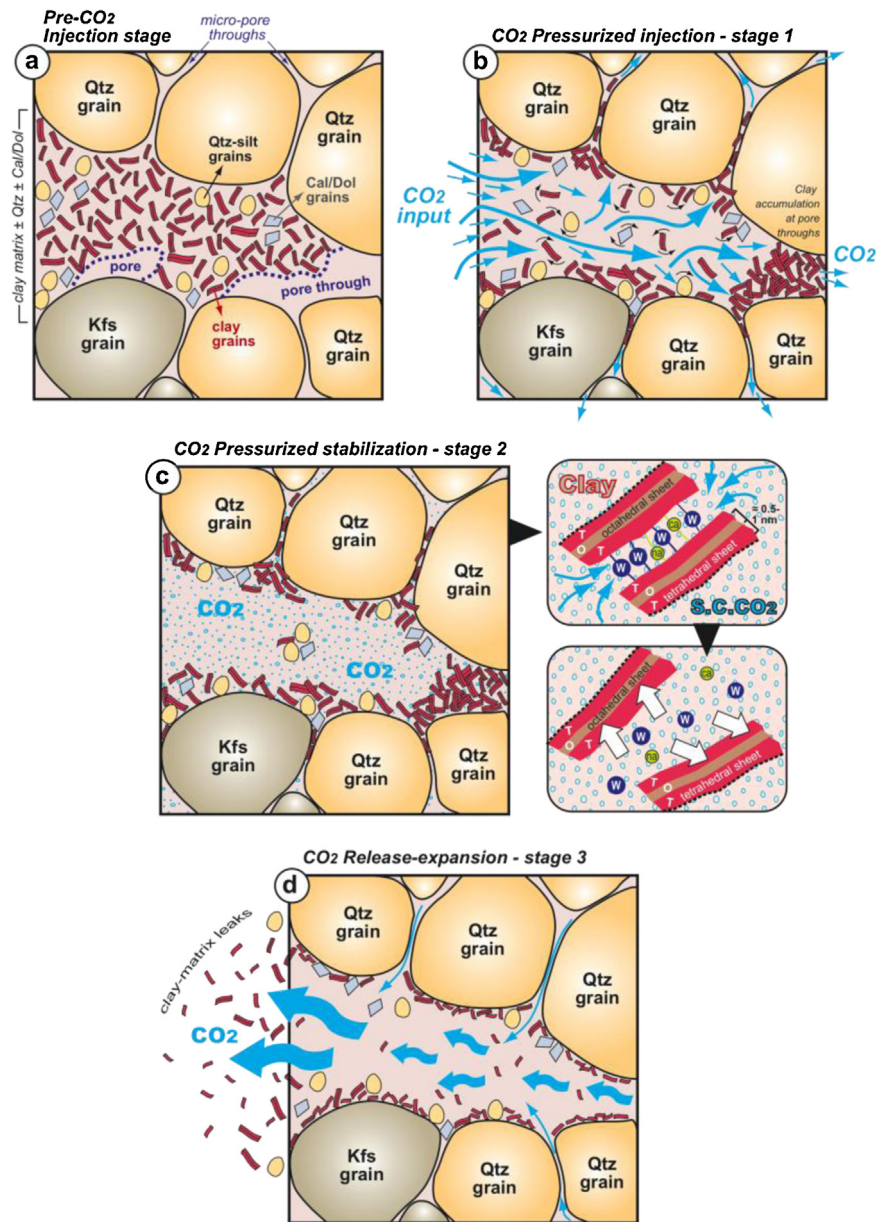


Fig. 8. Sketch drawings of the model developed from the observed mineralogy/textural changes, after the S.C. CO₂ experimental injection in the sandstone samples. In sketch (a) the initial mineralogy and texture of the sandstones is depicted. Clay matrix partially fills some intergranular spaces. When the CO₂ pressurized injection begins, (b), the gas drag force breaks inter-clay particle physical bonds and pulls the clay particles towards pore throats. During the longest experimental stage, (c), the pressurized CO₂ diffuses into clay layered structures, producing changes in the interlayer electrical forces that lead to inter-clay layer repulsion and break up (scale bar – 0.5–1 nm – is only for the approximate size of the interlayer structure of the clay). When the pressure releases, in the end-stage of the experiment, (d), CO₂ expands and generates further intra-clay particle break up, plus an outwards drag force that causes leaks and explains the observed matrix-clay absence in the samples after the experiment.

- CO₂ expansion during pressure release migrates from the pore troughs outwards, causing a physical clay outburst pulling out the clays from their location within the pores and pore troughs. This drag outwards effect would explain the partial loose of the clay matrix in the sample outer domains, as observed in the processed samples for optical and SEM studies (Fig. 8d).

This model permits us to explain the observed absence/modal reduction of the clay matrix in the studied rock samples (optical and SEM processed samples). Initially, it was thought that the loose matrix from the post-CO₂ samples have been partially leaked during sample processing. Nevertheless, the absence of matrix in the SEM samples, with minimal processing, was not well explained in this way. In the proposed model, the last stage (Fig. 8d – stage 3-) of

pressure release and gas expansion could have generated drag outwards forces that probably favoured partial leaks of the loose clays located near the sample edges. The low amount of the rock sample and the small grain size of these clay particles probably prevent us from observe them in the reactor chamber site.

No dissolution processes are expected because no water was available (or its wt.% was insignificant) and no new precipitated minerals were observed in the treated samples. Nevertheless, some studies have shown the possibility of Si dissolution because SC. CO₂ can act as a reliable solvent for some elements (Remoroza et al., 2012). This could have promoted partial clay dissolution. In this case, dissolved clay components would have had precipitated when pressure release ended the SC state of CO₂ (stage 3). These precipitated products were not observed in our study cases, and therefore,

either the experimental run time was not enough for this process to be effective, or the amount of dissolved-precipitated clays was very small to be easily observed.

In internal domains of the rock sample part of the loose clay matrix probably remains, but a complete or partial matrix grain re-adjustment has taken place. This indicates that the clay particles that form part of this matrix have moved and were detached from each other and, partially, from the major grains. This also implies that the major mineral grains have also moved relatively to each other causing an overall porosity increase, but also, in some cases, a partial porosity decrease due to the fact that some Qtz grains become in touch with each other (Figs. 4 and 5). This hypothesis has implications for the measured porosity (observed by optical microscopy and SEM on thin sections) in the CO₂-treated samples.

In the injection realm, loose clay particles (produced by the CO₂ input) could agglomerate and plug part of the pore space thus reducing porosity and permeability. Nevertheless we consider this unlikely because: (i) the size of the clay particles has been probably reduced: break of interatomic layers by the CO₂-induced electrical-polarity forces. The small sized clays and nanoclays generated are less likely to plug pore space (ii) in our rock experiments no single pore or pore channel was observed to be filled or partially plugged with clays after the CO₂ input.

(ii) Carbonate cement stability

An important result is the remarkable stability of the carbonate cement compared with the clay matrix. Both in the homogeneous and heterogeneous sandstones the domains with abundant carbonate cements remain similar in the treated samples compared to the untreated ones. No appreciable differences are detected in the observations at different scales (optical microscopy and SEM). This indicates that the CO₂ mechanical drag force was not strong enough to break physical bonds between the carbonate particles that made the cement and also between these particles and major mineral grains such as Qtz. The absence of available pore water allows this stability of the carbonate cements and precludes its dissolution in acid CO₂ enriched brines (Sterpenich et al., 2009). Therefore, there is a quite different rheological behaviour between the clay matrix and the carbonate cements suggesting that, when dry CO₂ is injected into the sandstone storage rocks, it would preferentially move along the zones rich in clay matrix leaving the carbonate cement domains very little affected or non-affected. If the distribution of carbonate cement/clay-matrix domains is not randomly disposed but occurs in an anisotropic framework such as a layering (carbonate cement and clay matrix in alternate layers) then the CO₂ would be able to develop marked lateral pathways which could increase the possibility for possible leaks.

(iii) Pore morphology variations after the CO₂ injection

In light of the previous hypothesis (clay matrix leaching induced by the CO₂) the measured porosity increases are experimental approximations that have to be reconsidered and interpreted in the context of the injection realm. The effects of CO₂ in the experimental rock system can have important influence on local and wide range parameters such as porosity and the general permeability. We also have shown that the original texture of the storage rocks is an important variable that could determine the intensity of the CO₂ induced changes (in mineralogy and texture).

In the SB homogeneous sandstone, the porosity data study (statistical test comparisons between pre-CO₂ and post-CO₂ rock samples, Table 1) shows that the CO₂ input produces significant changes in the pore area (calculated p values $< \alpha: 0.1 \Rightarrow$ we can reject the null hypothesis of mean equality \rightarrow pre-CO₂ \neq post-CO₂) while no change in the aspect ratio of the pores occur

(calculated p values $> \alpha: 0.1$, precluding the rejection of the null hypothesis \rightarrow pre-CO₂ = post-CO₂). This could indicate that the estimated increase in porosity (3%; Table 1) from the pre-injection to the post-injection samples was mainly due to generation of new pores and not to the increase of the previous porosity. This hypothesis is suggested because a process of pore growth from previous porosity (such as partial dissolution of pore-edge mineral phases) would probably modify the aspect ratio of the original pores: pores are surrounded by different mineral phases with different physical-chemical properties and pore growth would take place at the expense of the space developed on these phases, some more stable than others.

Both in SB (homogeneous) and SI (heterogeneous) the roughness of the pore boundaries (fractal dimension) is significantly different in the pre- and post-CO₂ injection samples (p values $< \alpha: 0.1$). The variations (decreases) of surface roughness in the CO₂-treated samples (Table 2) are probably caused by the polish of the major grain surface due to friction/abrasion produced by the CO₂ mobilization of matrix clay and micron sized Qtz particles. As previously proposed, the gas input and release drag forces, aided by other intra-particle physic-chemical forces (electrical polarity changes), generated the detachment of the clay particles from each other and from the larger mineral grains and these mobilized particles caused an abrasive effect on the surface of mineral grains along the pores. Therefore, the CO₂-induced abrasive effect was probably enhanced in the heterogeneous SI sandstone (higher roughness decrease) due to the existence of a micro-channel network partially filled with clays where the gas flux was probably focussed. On the other hand, in the homogeneous SB sandstone (slightly lower roughness decrease) the circulation of CO₂ was not focused in narrow micro-channels but percolated through all the rock volume thus reducing the intensity of the clay particle re-mobilization. In this case, the CO₂ injection would have caused some particle re-mobilization, but as the intensity of this effect was not high enough, did not lead to highly polished grain surfaces, as in the case of the heterogeneous sandstone (SI).

Surface pore area increase in SI sandstone is observed by optical and scanning electron microscopy (Figs. 5 and 6). The statistical p values are close to 0 (Table 1) and thus lower than the critical threshold value ($\alpha: 0.1$) indicating significant increase of the pore area. The aspect ratio of the pores increases after the CO₂ injection and the roughness and circularity show a significant decrease. Some of these parameters do not show the variation expected: the samples exposed to CO₂ injection develop pores with less roughness and acquire less circular shapes. This could indicate that the increase of porosity in the CO₂ treated SI sample ($\Delta n \sim 4\%$; Table 1) is due to the growth-increase of the previous pores. Such a process could have polished the pore surfaces, reduce its circularity and modify its aspect ratio.

Both these textural parameters (circularity and aspect ratio) should change in a connected way: if circularity increases, then the aspect ratio should approach 1 (decrease in the log data of Table 2). This expected behaviour is well matched in the case of the pores: in the SB sample circularity does not change and neither does the aspect ratio. In the SI pores, a circularity decrease is matched by an aspect ratio increase.

5. Conclusions

Experimental supercritical (S.C.) CO₂ injection into sandstone rock samples that represent appropriate storage formations simulates the interaction of rock-gas in dry conditions. Such environment is expected near the injection well environment during the initial stages of CO₂ deep injection. Our study indicates significant changes in the rock system caused by this dry CO₂ injection.

Mineral–chemical reactions were not detected in the sandstones after the CO₂ input due to the absence of water, or its presence in a very low amount.

The major change observed is a notable reduction of the modal clay–matrix that also leads to an increase of the measured porosity in the thin sections studied. The clay particles were detached from each other and from the major mineral grains and re-mobilized by the CO₂ effects. These were gas input–release drag forces and probably, as observed by other authors, interparticle electrical/physical forces activated by the CO₂ diffusion within the clay layered structures (During Stage 2 – CO₂ pressurized stabilization). This texture re-adjustment caused by the clay particle mobilization should always generate pore-network re-adjustments that in some domains could enhance permeability and in others could seal it. Partial clay matrix leaks were due to outward drag forces during gas expansion at the pressure release phase of the experiments. Further studies on porosimetry with indirect techniques, or less interactive ones, are necessary to quantify porosity variations after the CO₂ injection and make more realistic comparisons with the injection environment.

- The indirect influence of the original rock texture is important and leads to different effects produced by the CO₂ injection. When the sandstone has heterogeneous micro-channel pore networks (SI sample), the CO₂ is preferentially focused into these channels and interacts strongly with these specific sites of the rock volume. When the sandstone has a more homogeneous texture and pore network (SB sample), the injected CO₂ percolates through all the rock volume, its interaction reaches much of the rock but the intensity of clay particle-remobilization is lower.
- In contrast to the clay matrix, carbonate cements are quite stable and no significant changes were detected after the CO₂ injection in the studied sandstones. This suggests that the physical binds among carbonate matrix grains and also with major mineral grains (mainly Qtz) is higher compared to those of matrix-clay particles. Sandstones with high to moderate porosity and predominant carbonate cements are expected to be very stable in the conditions of dry- CO₂ S.C. injection. On the other hand, sandstones with high to moderate pore abundances and predominant clay matrix will be unstable for CO₂ injection in dry conditions. Furthermore, if the pore framework of the potential storage sandstone is highly anisotropic (i.e., channel-microstructures) more pronounced textural changes are to be expected.

The observed experimental textural and mineralogical changes can have significant effects in the environment around injection wells: in this zone, the CO₂ will probably act like a piston, pressing and displacing the brine fluids from the storage rock pores without mixing and thus the injected CO₂ will be in contact with the rock framework in dry conditions. In this scenario, dry gas–rock interactions become important for the stability of the storage rock and the injection well. The CO₂ input can force aside the particles by its drag pressure further modifying the texture and pore framework (Fauria and Rempel, 2011). The observed textural and mineralogical changes that led to the porosity and permeability changes could also ease the CO₂ further injection. Nevertheless, the main change observed in this study is a textural–mineralogical re-adjustment of the matrix clay within the rock framework.

Acknowledgments

Funding from CO₂–Pore Project (Plan Nacional de España: 2009-10934), ALGEC02 Project (Instituto Geológico y Minero de España), Minería XXI Project (CYTED: 310RT0402) and ADI-CO₂ Project (CIUDEN: ALM/12/028) are greatly appreciated. We would also like to

thank to Laura Arenas, Peter Olaya, Israel Perez, Roberto Martinez, José Luis García Lobón and Félix Mateos for providing help in DIA techniques, data acquisition, statistical treatment and rock sample collection. We acknowledge Stefan Bachu for editorial handling and two anonymous reviewers for their constructive comments and corrections.

Appendix 1. Software references

APHELION IMAGING SOFTWARE SUITE for Windows. Version 3.2. [Processing and Image Analysis Software]. ADCIS, Inc., Available in <http://www.adcis.net/>.

HEL for Windows. Version 5.1 [WinISO Software Control System Reactor] Available in <http://www.helgroup.com/reactor-systems/chemical-reactors/>.

IMAGE-PRO PLUS for Windows. Version 7.0. [Image Analysis Software]. Media Cybernetics, Inc., Available in <http://www.mediacy.com/index.aspx?page=IPP>.

INCA ENERGY. Version 200. [Energy Dispersive Spectrometry (EDS) System]. Oxford Instruments Analytical. Available in <http://www.oxford-instruments.com/>.

MINITAB for Windows. Version 15.0. [Statistical Software]. Available in <http://www.minitab.com/es-ES/products/minitab/>.

SYSTAT for Windows. Version 13.0. [Statistical Analysis and Graphics Software]. Available in <http://www.systat.com/SystatProducts.aspx>.

Appendix 2. Mineral symbols (after Kretz, 1983)

Ap. Apatite
 Bt. Biotite
 Cal. Calcite
 Chl. Chlorite
 Dol. Dolomite
 Kfs. K Feldspar
 Ms. Muscovite
 Pl. Plagioclase
 Qtz. Quartz
 Tur. Tourmaline
 Zrn. Zircon

References

- Andreani, M., Gouze, P., Luquot, L., Jouanna, P., 2008. Changes in sealing capacity of fissured claystone caprocks induced by dissolved and gaseous CO₂ seepage. *Geophysical Research Letters* 35, <http://dx.doi.org/10.1029/2008GL034467>.
- Azcárate Martín, J.E., Esnaola Gómez, J.M., Maldonado, M., 1974. Hoja 1:50.000 de Linares (N° 905). In: Plan MAGNA. IGME, España.
- Bacci, G., Korre, A., Durucan, A., 2011. An experimental and numerical investigation into the impact of dissolution/precipitation mechanisms on CO₂ injectivity in the wellbore and far field regions. *International Journal of Greenhouse Gas Control* 5 (3), 579–588.
- Benson, S.B., Cole, D.R., 2008. CO₂ sequestration in deep sedimentary formations. *Elements* 4, 325–331.
- Berrezueta, E., Castroviejo, R., 2007. Automated microscopic characterization of metallic ores with image analysis: a key to improve ore processing. I: test of the methodology. *Revista de Metalurgia Madrid* 43 (4), 294–309.
- Berrezueta, E., Olaya, P., Arenas-Montes, L., Bernhardt, R., 2012. DIA computer applications to quantify mineralogical parameters: adjustment of equipment and development algorithms. In: Berrezueta, E., Dominguez-Cuesta, M.J. (Eds.), *Técnicas aplicadas a la caracterización y aprovechamiento de recursos geológico-mineros*, vol. 3. IGME, Oviedo, Spain, pp. 17–27.
- Burton, M., Kumar, K., Bryant, S.L., 2008. Time-dependent injectivity during CO₂ storage in aquifers, in *Symposium on Improved Oil Recovery*, 20–23 April 2008, Tulsa, Okla., 2008. In: *Proceedings: Richardson, Tex., Society of Petroleum Engineers*, paper SPE 113937, p. 15, <http://dx.doi.org/10.2118/113937-MS>.
- Cailly, B., Le Thiez, P., Egermann, P., Audibert, A., Vidal-Gilbert, S., Longaygue, X., 2005. Geological storage of CO₂: a state-of-the-art of injection processes and technologies. *Oil and Gas Science and Technology – Revue de l'IFP* 60 (3), 517–525.
- Desbois, G., Urai, J., Kukla, P., Konstanty, J., Baerle, C., 2011. High-resolution 3D fabric and porosity model in a tight gas sandstone reservoir: a new approach to investigate microstructures from mm- to nm-scale combining argon beam

- cross-sectioning and SEM imaging. *Journal of Petroleum Science and Engineering* 78 (2), 243–257.
- Egermann, P., Bazin, B., Vizika, O., 2005. An experimental investigation of reaction-transport phenomena during CO₂ injection. In: Paper SPE 93674, presented at The SPE Middle East Oil Show, Bahrain, 12–15 March.
- Espinoza, N.D., Santamaría, J.C., 2012. Clay interaction with liquid and supercritical CO₂: the relevance of electrical and capillary forces. *International Journal of Greenhouse Gas Control* 10, 351–362.
- Fauria, E., Rempel, A., 2011. Gas invasion into water-saturated, unconsolidated porous media: implications for gas hydrate reservoirs. *Earth Planetary Science Letter* 312 (1/2), 188.
- Folk, R.L., 1974. *The Petrology of Sedimentary Rocks*. Hemphill Publishing Co., Austin, TX, pp. 182.
- Fripiat, J.J., Cruz, M.I., Bohor, B.F., Thomas, J., 1974. Interlamellar adsorption of carbon dioxide by smectites. *Clays and Clays Minerals* 22, 23–30.
- Gauss, I., Audigane, P., Andre, L., Lions, J., Jacquement, N., Durst, P., Czernichowski, I., Azaroual, M., 2008. Geochemical and solute transport modelling for CO₂ storage, what to expect from it? *International Journal of Greenhouse Gas Control* 2, 605–625.
- Gauss, I., 2010. Role and impact of CO₂–rock interactions during CO₂ storage in sedimentary rocks. *International Journal of Greenhouse Gas Control* 4, 73–89.
- Gunter, W.D., Bachu, S., Benson, S., 2008. The Role of Hydrogeological and Geochemical Trapping in Sedimentary Basins for Secure Geological Storage of Carbon dioxide, vol. 233. Geological Society, London, pp. 129–145.
- Horsch, S., Sehatkulu, G., Gulari, E., Kannan, R.M., 2006. Supercritical CO₂ dispersion of nano-clays and clay/polymer nanocomposites. *Polymer* 47, 7485–7496.
- Izeg, O., Demiral, B., Bertin, H., Akin, S., 2008. CO₂ injection into saline carbonate aquifer formations I: laboratory investigation. *Transport in Porous Media* 72, 1–24.
- İzgeç, Ö., Demiral, B., Bertin, H., Akin, S., 2005. Experimental and numerical investigation of carbon sequestration in deep saline aquifers. In: Paper SPE 94697, SPE/EPA/DOE Exploration and Production Environmental Conference to be held, Galveston, Texas, 7–9 March.
- Kharaka, Y.K., Cole, D.R., Hovorka, S.D., Gunter, W.D., Knauss, K.G., Freifeld, B.M., 2006. Gas–water–rock interactions in Frio formation following CO₂ injection: implications for the storage of greenhouse gases in sedimentary basins. *Geology* 34–37, 577–580.
- Kaszuba, J.P., Janecky, D.R., Snow, M.G., 2003. Carbon dioxide reaction processes in a model brine aquifer at 200 °C and 200 bars: implications for geologic sequestration of carbon. *Applied Geochemistry* 18, 1065–1080.
- Kaszuba, J.P., Janecky, D.R., Snow, M.G., 2005. Experimental evaluation of mixed fluid reactions between supercritical carbon dioxide and NaCl brine: relevance to the integrity of a geologic carbon repository. *Chemical Geology* 217, 277–293.
- Kretz, R., 1983. Symbols for rock-forming minerals. *American Mineralogist* 68, 277–279.
- Lendínez González, A., Muñoz del Real, J.L., 1989. Hoja 1:50,000 de Berlanga de Duero (N° 405). In: Plan MAGNA. IGME, España.
- Luquot, L., Gouze, P., 2009. Experimental determination of porosity and permeability changes induced injection of CO₂ into carbonate rocks. *Chemical Geology* 265, 148–159.
- Luquot, L., Andreani, M., Gouze, P., Camos, P., 2012. CO₂ percolation experiment through chlorite/zeolite-rich Hill Formation – Otway Basin – Australia. *Chemical Geology* 294/295, 77–88.
- Mito, S., Xue, Z., Ohsumi, T., 2008. Case study of geochemical reactions at the Nagaoka CO₂ injection site, Japan. *International Journal of Greenhouse Gas Control* 2, 309–318.
- Pèpe, G., Dweik, J., Jouanna, P., Gouze, P., Andreani, M., Luquot, L., 2010. Atomic modelling of crystal/complex fluid /crystal contacts – Part II. Simulating AFM tests via the GenMol code for investigating the impact of CO₂ storage on kaolinite/brine /kaolinite adhesion. *Journal of Crystal Growth* 32, <http://dx.doi.org/10.1016/j.jcrysgro.2010.08.012>.
- Perkins, E.H., Gunter, W.D., 1995. Aquifer disposal of CO₂-rich greenhouse gases: modeling of water–rock reaction paths in a siliciclastic aquifer. In: Kharaka, Y.K., Chidaev, O.V. (Eds.), *Water-Rock Interactions*. Brookfield, Rotterdam, pp. 895–898.
- Pettijohn, F.J., Potter, P.E., Siever, R., 1973. *Sand and Sandstones*. Springer-Verlag, New York/Heidelberg, Berlin, pp. 618.
- Remorosa, A., Doroodchi, E., Moghtaderi, B., 2012. CO₂-EGS in hot dry rock: preliminary results from CO₂–rock interaction experiments. In: Thirty-Seventh Workshop on geothermal Reservoir Engineering Stanford University, January 30–February 1, SGP-TR-194, Stanford, CA.
- Rochelle, C.A., Czernichowski, L., Milodowski, A.E., 2004. The Impact of Chemical Reactions on CO₂ Storage in Geological Formations: A Brief Review. Geological Society, London, pp. 87–106.
- Ross, G.D., Todd, A.C., Tweedie, J.A., Will, A.G.S., 1982. Dissolution effects of CO₂-brine systems on the permeability of UK and North Sea calcareous sandstones. In: Paper SPE/DOE 10685. Presented at the 1982 SPE/DOE Symposium on Enhanced Oil Recovery, April 4–7, Tulsa, Oklahoma.
- Saeedi, A., Rezaee, R., Evans, B., Clennell, B., 2011. Multiphase flow behaviour during CO₂ geo-sequestration: emphasis on the effect of cyclic CO₂–brine flooding. *Journal of Petroleum Science and Engineering* 79 (3/4), 65–85. <http://dx.doi.org/10.1016/j.petrol.2011.07.007>.
- Sayegh, S.G., Krause, F.F., Girard, M., 1990. Rock/fluid interactions of carbonated brines in a sandstone reservoir Pembina Cardium, Alberta, Canada [J]. *SPE Formation Evaluation* 5 (4), 399–405.
- Sterpenich, J., Sausse, J., Pironon, J., Géhin, A., Hubert, G., Perfetti, E., Grgic, D., 2009. Experimental ageing of oolitic limestones under CO₂ storage conditions. Petrographical and chemical evidence. *Chemical Geology* 265, 99–112.
- Svec, R.K., Grigg, R.B., 2011. Physical effects of WAG fluids on carbonate core plugs. In: Paper SPE 71496 presented at The Annual Technical Conference and Exhibition, Soc. of Pet. Eng. New Orleans, La, 30 September–3 October.
- Vickerd, M.A., Thring, R.W., Arocena, J.M., Li, J.B., 2006. Changes in porosity due to acid gas injection as determined by X-ray computed tomography. *Journal of Canadian Petroleum Technology* 45 (8), 17–22.